An Interfacial Stress Rheometer To Study Rheological Transitions in Monolayers at the Air–Water Interface

ARTICLE *in* LANGMUIR · MARCH 1999

Impact Factor: 4.46 · DOI: 10.1021/la980465r

4 AUTHORS, INCLUDING:

Carlton F. Brooks
Sandia National Laboratories
45 PUBLICATIONS **546** CITATIONS
SEE PROFILE

Curtis W. Frank
Stanford University
363 PUBLICATIONS **9,963** CITATIONS
SEE PROFILE

An Interfacial Stress Rheometer To Study Rheological Transitions in Monolayers at the Air−Water Interface

Carlton F. Brooks, Gerald G. Fuller,* Curtis W. Frank, and Channing R. Robertson

Department of Chemical Engineering, Stanford University, Stanford, California 94305-5025

Received April 23, 1998. In Final Form: December 31, 1998

An interfacial stress rheometer has been constructed to study the rheology of Langmuir films subjected to time-dependent flows. A magnetized rod resides at the air−water interface and is set into oscillation by applying a sinusoidal magnetic field gradient. Analysis of the amplitude and phase of the resulting rod motion relative to the applied force allows the determination of the dynamic surface modulus, $G_s^*(\omega)$, and measurement of the relative elastic and viscous contributions of the monolayer. Measurements at 22 °C were conducted on eicosanol (C_{20}) and mixtures of a rigid-rod polymer, phthalocyaninatopolysiloxane (PcPS), dispersed in eicosanol. The surface pressure dependence of the rheology for eicosanol reveals the presence of a maximum in the loss modulus, $G_s''(\omega)$, within the L_2' phase at $\Pi = 6$ mN/m. In the LS_I phase at pressures above 15 mN/m, the monolayer is Newtonian and has a surface viscosity of 0.03 mN·s/m. The mixtures of PcPS with eicosanol are known to have two-dimensional nematic behavior. The presence of PcPS in the film increased $||G_s^*(\omega)||$ 100-fold, creating a non-Newtonian interface with a measurable elasticity. As the polymer rod concentration was increased further, $G_s^*(\omega)$ became less dependent on frequency, and above the isotropic−nematic transition, the storage modulus, $G_s'(\omega)$, exceeded the loss modulus, $G_s''(\omega)$. The results on eicosanol and the mixtures of the rigid rod with eicosanol demonstrate that the rheometer is capable of detecting microstructural transitions in a Langmuir monolayer.

Introduction

The rheology of monolayers of insoluble surfactants at the air−water interface has been a subject of research interest for many years. Even though very little effort is needed to deform these molecularly thin films, the capability of measuring the force necessary to shear the film (at different deformations, γ, and deformation rates, $\dot{\gamma}$) and comparing them at different thermodynamic conditions (temperature, T, and surface pressure, Π) can provide valuable information beyond that obtained with pressure−area isotherms. Knowledge of the flow behavior of these films can provide insight into molecular interactions under dynamic conditions, e.g., hydrogen bonding between neighboring molecules, physical entanglements, covalent cross-linking, etc. This understanding could be useful for the physical scientist seeking to understand molecular forces in a confined geometry or the applications engineer transferring molecular films to solid substrates by Langmuir−Blodgett deposition.

Several different devices have been proposed to measure the forces to deform these delicate films, including canal devices,[1] channel flow devices,[2,3] rotating disks and rings,[4−8] and knife-edge devices.[9,10] Each device has been reviewed in the literature.[11−14] One of the main goals in the design of these instruments is to provide adequate sensitivity to detect stresses in the surface film in the presence of stresses from the underlying subphase.[13−15] To describe the extent of the interaction of the monolayer with the subphase, a dimensionless ratio of the two components of the drag experienced by the rheological probe can be formed

$$Bo \equiv \frac{\text{surface drag}}{\text{subphase drag}} = \frac{\mu_s \frac{V}{L_c'} P_c}{\mu \frac{V}{L_c''} A_c} = \frac{\mu_s}{\mu} \frac{P_c}{A_c} \frac{L_c''}{L_c'} \qquad (1)$$

where Bo is the Boussinesq number.[14] Here, μ is the subphase viscosity, μ_s is the surface viscosity, V is a characteristic velocity, L_c' and L_c'' are the characteristic length scales in which the velocity decays in the surface and subphase, respectively, P_c is the contact perimeter between the rheological probe and the interface, and A_c is the contact area between the probe and the subphase. When $Bo \gg 1$, the drag experienced by the probe predominantly arises from the surface; when $Bo \ll 1$, the subphase flow properties are measured. The ratio of P_c to A_c is the simplest experimental parameter to vary that will increase the sensitivity to surface stresses. This ratio is at a *minimum* for the rotating disk ($P_c/A_c = 4/D$, where D is the disk diameter), which limits its range of sensitivity to very rigid films. A rotating disk that is 30 mm in diameter will have a ratio of 0.13 mm^{-1}. Ring or knife-

(1) Mannheimer, R. J.; Schechter, R. S. *J. Colloid Interface Sci.* **1970**, *32*, 225.
(2) Sacchetti, M.; Yu, H.; Zografi, G. *J. Chem. Phys.* **1993**, *99*, 563.
(3) Kurnaz, M. L.; Schwartz, D. K. *Phys. Rev. E* **1997**, *56*, 3378.
(4) Gaub, H. E.; McConnell, H. M. *J. Phys. Chem.* **1986**, *90*, 6830.
(5) Camtel Ltd., U.K., web site, http://www.camtel.co.uk/, 1998.
(6) Abraham, B. M.; Miyano, K.; Ketterson, J. B.; Xu, S. Q. *Phys. Rev. Lett.* **1983**, *51*, 1975.
(7) Krägel, J.; Siegel, S.; Miller, R.; Born, M.; Schano, K.-H. *Colloids Surf. A* **1994**, *91*, 169.
(8) Ghaskadvi, G. H.; Ketterson, J. B.; MacDonald, R. C.; Dutta, P. *Rev. Sci. Instrum.* **1997**, *68*, 1792.
(9) Goodrich, F. C.; Allen, L. H.; Poskanzer, A. *J. Colloid Interface Sci.* **1975**, *52*, 201.
(10) Gordon T. Shahin, Ph.D. thesis, The University of Pennsylvania, 1986.
(11) Goodrich, F. C. In *Progress in Surface and Membrane Science*; Danielli, J. F., Rosenberg, M. D., Cadenhead, D. A., Eds.; Academic Press: New York, 1973; Vol. 7, p 151.
(12) Warburton, B. *Curr. Opinion Colloid Int. Sci.* **1996**, *1*, 481.
(13) Joly, M. In *Surface and Colloid Science*; Matijevic, E., Ed.; Wiley-Interscience: New York, 1972; Vol. 5, p 1.
(14) Edwards, D. A.; Brenner, H.; Wasan, D. T. *Interfacial Transport Processes and Rheology*; Butterworth-Heinemann: Boston, 1991; Chapter 7.
(15) Stone, H. A. *Phys. Fluids* **1995**, *7*, 2931.

10.1021/la980465r CCC: $18.00
Published on Web 03/11/1999

edge probes are optimal since $P_c/A_c \sim O(1/a)$, where a is the thickness of the knife edge. For the magnetic rod probe used in this work (33 mm long × 0.450 mm in diameter), this ratio is 2.8 mm^{-1}.

Here we present the design of an interfacial stress rheometer that can be used to apply a shear stress to a Langmuir monolayer and monitor the time-dependent response of the rheological probe, which is a magnetic rod. It has the following advantages when compared to other existing techniques: (1) the interfacial stresses can be measured in real time, allowing the study of time-dependent flows and, subsequently, the determination of the elasticity and viscosity of the monolayer; (2) the frequency of the applied force can be readily changed without having to change the elements of the rheometer, e.g., the torsion wire in some of the torsion−bob-based devices;[6,7] (3) the strain rate is determined from the position of the rod, avoiding the need to use tracer particles to analyze velocity profiles, as is required in the deep channel surface viscometer;[1] (4) non-Newtonian surfaces can be examined since no assumptions regarding the constitutive behavior are required to analyze the flow response, which is required for some channel flow methods;[2] (5) there is high sensitivity to surface stresses in the presence of bulk subphase stresses due to the high P_c/A_c ratio for the magnetic rod; and (6) the surface pressure and temperature can be readily changed without having to change the geometry of the flow cell.[8]

To verify that the surface rheometer described here is a tool capable of detecting microstructural changes in monolayers, rheological data at 22 °C are presented on the fatty alcohol eicosanol and a well-studied monolayer mixture of this fatty alcohol with a rigid-rod polymer, phthalocyaninatopolysiloxane (PcPS).[16,17]

Monolayers of saturated fatty acids and alcohols have been thoroughly investigated, and from X-ray diffraction studies, a considerable amount is known about the structure within these films.[18] Recent rheological studies by Ghaskadvi et al.[19] on heneicosanoic acid (C_{21}) have correlated a maximum in the loss modulus with a change in lattice structure. By using a surface rheometer based on a knife-edge torsion pendulum design, they were able to measure the storage and loss moduli of a Langmuir film (G_s' and G_s'', respectively). A maximum was found for G_s'' in the L_2 phase, where, in general, the molecules are arranged on a distorted hexagonal lattice and are tilted toward their nearest neighbors (NN). X-ray studies have showed that although the lattice structure is predominantly distorted hexagonal within the L_2 phase, there is a unique surface pressure at which the lattice is undistorted. The maximum in G_s'' was correlated with this undistorted lattice structure; however, Ghaskadvi et al. never concluded that this packing was the cause for the observed rheological response. In the present work, we examine the rheology of the C_{20} alcohol, eicosanol, along its 22 °C isotherm as it goes from the low-pressure L_2' phase, where the molecules are positioned on a distorted hexagonal lattice with next-nearest-neighbor (NNN) tilt, to the LS_I phase, where the molecules are untilted, arranged on a hexagonal lattice, and have increased rotational mobility about the chain axis. We observed a low-pressure maximum in G_s'' for eicosanol within the L_2' phase, similar to what Ghaskadvi et al. observed in the L_2 phase of heneicosanoic acid, and a pressure-induced liquefaction at the L_2'−LS_I transition as the surface changes from a NNN tilted polydomain to an untilted Newtonian surface. This last transition was observable using Brewster angle microscopy (BAM).

Solutions of rigid rods in a Newtonian solvent are an excellent model system to measure the shear rheology because they behave as lyotropic liquid crystals. In our laboratory, we have investigated the orientation dynamics of a monolayer of the rigid-rod polymer PcPS in the Newtonian, LS_I phase of eicosanol and have been very successful at modeling it as a two-dimensional nematic.[16,17] If c is the number of rods per unit surface area and L_p is the length of a polymer rod, then three concentration regimes can be derived from simple scaling arguments: at low concentrations, the rods are isotropic, $cL_p^2 \ll 1$; at intermediate concentrations, they are isotropic semidilute, $1 < cL_p^2 < U^*$; and at high concentrations, they are nematic, $cL_p^2 > U^*$, where U^* is the dimensionless concentration at which the isotropic−nematic transition occurs. From 2D models of rigid rods using a nematic potential,[17,20] the transition has been predicted to occur for $U^* = 2-2.35$. The Doi−Hess model predicts that in three dimensions, a semidilute suspension of rods under steady shear has an elastic component of the stress that scales with c^3 and a viscous component that scales with c. Once the rods enter the nematic phase, the rotational diffusivity increases, causing the viscosity to *decrease* with increasing rod concentration. The Doi−Hess[21−24] rigid-rod model predicts that the viscosity should continue to decrease with concentration. Experiments with suspensions of rigid helical polypeptides,[25] however, reveal that after the viscosity decreases with concentration, it can increase further because of more rod−rod interactions. The system reaches a point where the degree of order is not significantly increased with additional rods. The benefits of a higher rotational diffusivity from better alignment are superseded by decreases in rod−rod separation. In the work described here, we found that the addition of rigid rods had a large effect on the rheology but a minimal effect on the isotherm. Transitions in the dynamic surface modulus were observed going from an isotropic to a nematic state in the rigid-rod polymer/alcohol mixture, in agreement with measurements of the molecular orientation with dichroism.[16,17]

Experimental Section

Interfacial Stress Rheometer (ISR). *Trough and Surface Pressure Measurement.* A commercial Langmuir trough made of Teflon was used for all measurements (KSV Instruments, Helsinki, Finland). The trough dimensions were 33.0 cm × 7.5 cm, and it was equipped with a quartz window (30 mm in diameter) flush with the bottom of the trough. Two hydrophillic barriers were moved symmetrically to change the surface concentration of the surfactant molecules at the interface. The surface pressure was monitored using a Wilhelmy balance.

Helmholtz Coils and Magnetic Field. Helmholtz coils were used to produce a constant magnetic field gradient. In this geometry, there is a pair of solenoid rings aligned along the same axis and separated by one ring radius. The trough was positioned

(16) Friedenberg, M. C.; Fuller, G. G.; Frank, C. W.; Robertson, C. R. *Macromolecules* **1996**, *29*, 705.
(17) Maffettone, P. L.; Grosso, M.; Friedenberg, M. C.; Fuller, G. G. *Macromolecules* **1996**, *29*, 8473.
(18) Kaganer, V. M.; Peterson, I. R.; Kenn, R. M.; Shih, M. C.; Durbin, M.; Dutta, P. *J. Chem. Phys.* **1995**, *102*, 9412.
(19) Ghaskadvi, G. H.; Ketterson, J. B.; Dutta, P. *Langmuir* **1997**, *13*, 5137.
(20) Marrucci, G.; Maffettone, P. L. *Macromolecules* **1989**, *22*, 4076.
(21) Doi, M.; Edwards, S. F. *The Theory of Polymer Dynamics*; Clarendon Press: Oxford, 1986; Chapters 8−10.
(22) Hess, S. *Z. Naturforsch. A* **1976**, *31A*, 1034.
(23) Doi, M. *J. Polym. Sci.: Polym. Phys. Ed.* **1980**, *19*, 229.
(24) Larson, R. G. *Constitutive Equations for Polymer Melts and Solutions*; Butterworths: Boston, 1988; Chapter 10.
(25) Kiss, G.; Porter, R.S. *J. Polym. Sci.: Polym. Phys. Ed.* **1980**, *18*, 361.

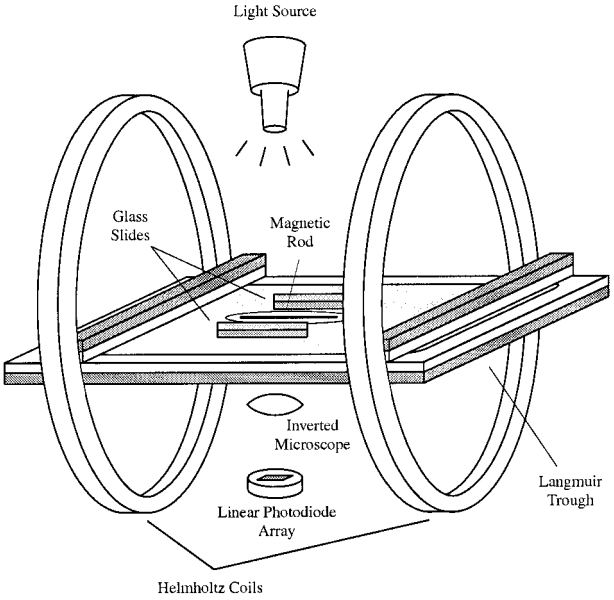

Figure 1. Schematic diagram of the magnetic rod interfacial stress rheometer (ISR) apparatus showing the main elements of the device (the support framework for these elements is withheld for clarity). A magnetized rod is supported by surface tension at the air−water interface inside a conventional Langmuir trough. The trough is surrounded by a pair of Helmholtz coils to create a magnetic field gradient, which applies a force on the rod to shear the film. It is assumed that the drag experienced by the rod predominantly arises from shear stresses developed between the glass slides and the rod. The position of the rod is detected by tracking the end of the needle. An inverted microscope, denoted by L for clarity, is focused on the end of the needle, and the resulting image is projected onto a photodiode array. A time-dependent force (surface stress) can be applied, and the time-dependent displacement (strain) can be followed.

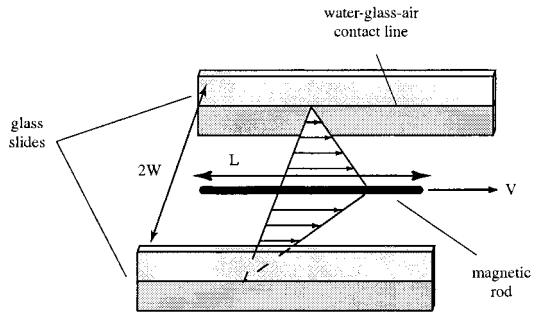

Figure 2. Close-up view of the magnetic rod between the glass slides of the flow cell (not to scale). The meniscus formed between the glass slides (not shown) aligns the rod along the centerline, and surface tension supports the rod.

so that the plane of the air−water surface was aligned with the axis (Figure 1). In our arrangement, two pairs of coils were used—one to apply the magnetic field gradient and the other to produce a constant magnetic field to fix the orientation of the rod with respect to the coil axis. The coil inductance, which can be used as a relative measure of the strength of the magnetic field generated by the coil, is 10 times larger for one pair compared to the other (110 mH vs 11 mH at 1 kHz). Even though only one pair is necessary, two pairs are convenient for covering a wider range of forces. Therefore, if measurements are being conducted on very viscous monolayers, the applied range of forces can be increased by choosing the pair of coils with the larger inductance to generate the magnetic field gradient. The forces that can be applied with the present design range from 0.001 to 30 μN. Two dc power supplies (Hewlett-Packard Model 6644A) were used to drive the pair of Helmholtz coils that generate the magnetic field gradient (Figure 3). The current setpoint of one of these power supplies was controlled with an analog signal from a function

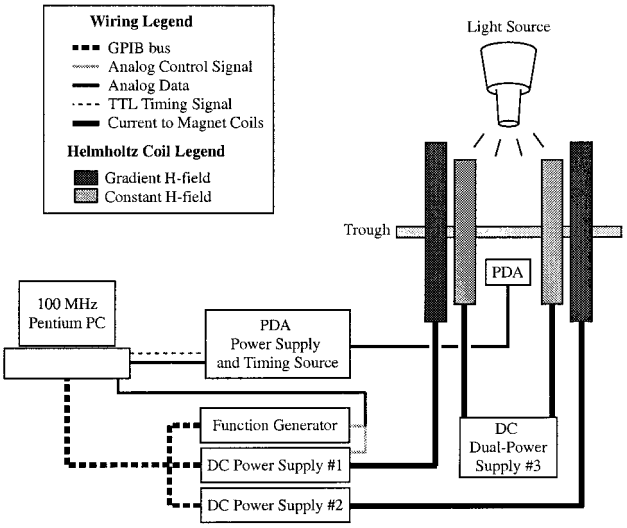

Figure 3. Sketch of the wiring diagram for the interfacial stress rheometer. The photodiode array (PDA) is used to image the rod's shadow, and the power supplies provide the current to produce the magnetic field. Two pairs of Helmholtz coils are used: one generates a uniform field (which aligns the rod and dominates any ambient magnetic fields) and the other a magnetic field gradient. The uniform field is used to align the rod and to dominate over any ambient magnetic fields. The magnetic field gradient is used to apply a force on the rod.

generator (Hewlett-Packard Model 3325B) to create a time-dependent magnetic field gradient. A third dc dual-power supply (Hewlett-Packard Model 6205C) was used to power the constant field coils.

Magnetic Rod and Flow Cell. The rheological probe for this surface rheometer is a magnetized rod residing between the two glass slides of the flow cell and floating at the air−water interface due to surface tension (Figure 2). The magnetic rod was located between the coils, where the magnetic field gradient is uniform. The magnetic rod used here was a needle with a radius, a, of 225 μm and a length, L, of 33 mm. Alternatively, more elegant magnetic rods can be made from thin magnetized iron wire. Thinner rods would be useful for increasing the dynamic range of the device, since at higher frequencies rod inertia decreases sensitivity. Thinner rods also increase sensitivity since the interfacial effects dominate over the bulk rheology of the subphase (Boussinesq number, $Bo \sim 1/a$). Unfortunately, reducing the rod diameter also reduces the amount of magnetic material per unit rod length; the force is proportional to a^2, resulting in a smaller force on a thinner rod for a given magnetic field gradient. Thus, although the sensitivity increases as a is decreased, reduction in the magnetization per unit rod length will require the use of very large magnetic fields, which becomes impractical. The magnetic rod was confined in a flow cell, which consisted of two partially submerged glass slides normal to the interface (Figure 2). The glass surfaces of the slides were mechanically roughened to aid in forming a straight contact line between the water, air, and glass. Straight contact lines were required for smooth motion of the rod. The hydrophillic nature of the slides produced a meniscus that aided in aligning the magnetic rod along the channel centerline, making it self-centering. The glass slides were supported by two thin Teflon blocks completely submerged in the subphase (not shown). Several block sizes were made for changing the gap separating the glass slides, $2W$, from 10 to 30 mm apart. Prior to each use, the glass slides were cleaned by immersing them in chloroform and sonicating them for at least 20 min.

Position Detection. The position of the rod was monitored as a function of time using a modified inverted microscope (Nikon Model TMS-F). Different combinations of objective and camera lenses on the microscope enabled attainment of the desired position sensitivity. The image was projected onto a linear image sensor with a 512-pixel photodiode array (Hamamatsu Model C4350 multichannel detector with Model S3902-512Q image sensor). Each pixel is 50 μm long (the total length of the line

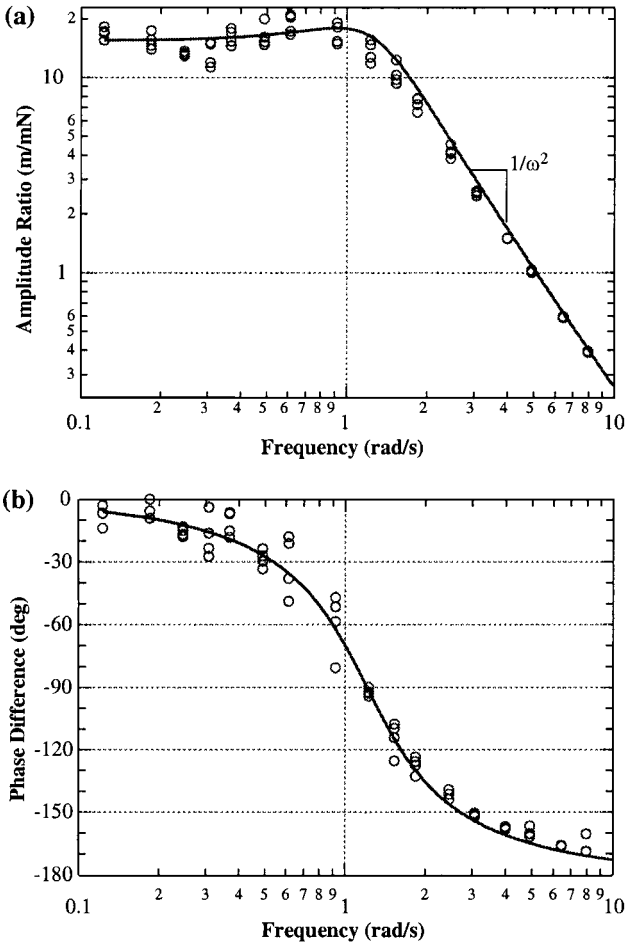

Figure 4. (a) Amplitude ratio and (b) phase angle as a function of forcing frequency for a clean air−water interface at $T = 15$ °C. The response behaves as a second-order system, with a low-frequency plateau, damped resonance peak, and inertial dampening at high frequencies ($AR \sim 1/\omega^2$). The strain lags the stress by 180° at high frequencies. The curve in a is the best fit to eq 2, and then these parameters are used in eq 3 to create the curve in b.

array is 25.6 mm) and 0.5 mm wide. The array output was analyzed to detect the edge of the rod. Figure 3 is a schematic diagram illustrating how the equipment communicated with the computer. With this arrangement, the position of the rod was obtained at a rate of 50 Hz with resolutions from 0.5 to 5 μm, depending on the optical arrangement.

System Frequency Characteristics and Force Calibration Method. Since one of the objectives of this research is to use this device to probe the rheological time spectrum of monolayers, a frequency sweep was conducted on a monolayer-free interface to see how the system behaved in the absence of a sample. In general, the system contribution depends on several variables, including the subphase viscosity, curvature of the magnetic field, and surface curvature in the direction of rod motion, as well as the rod inertia and dimensions.

The two parameters that are monitored are the amplitude ratio, AR, defined as the ratio of the amplitude of the rod displacement to the forcing amplitude, and the phase difference, δ, which is the difference between the rod response and the applied force. These were determined from the frequency spectrum obtained by taking the fast Fourier transform (FFT) of the applied force and the response of the rod.

In Figure 4, the response for water at 15 °C, AR_{system} and δ_{system}, is shown as a function of forcing frequency. In the absence of a monolayer, the dynamics of the rod motion can be characterized as a second-order system, with a low-frequency plateau, a damped resonance peak around 1 rad/s, and inertial dampening at high frequencies. The low-frequency plateau arises from the constant-current positioning coils since the potential well it creates is used to position the rod on the detector. The observed resonance arises due to the low viscosity of the water subphase. The overall frequency behavior can be described by

$$AR_{system} \equiv \frac{\text{rod position amplitude}}{\text{force amplitude}} = \frac{1}{\sqrt{(k - m\omega^2)^2 + (\omega d)^2}} \tag{2}$$

and

$$\delta_{system} \equiv \arctan\left(\frac{-\omega d}{k - m\omega^2}\right) \tag{3}$$

The three parameters k, d, and m are reference parameters used to describe the response of the device and are analogous to a spring constant, damping coefficient, and a mass, respectively. Since the only object in motion is the rod, m is the mass of the rod.

In actuality, the measured amplitude ratio is in units of distance per current (since it is the current difference between the coils that is responsible for generating the force on the rod). The units of current must be converted to units of force to compare the results from this device with other devices. The force on the rod is calibrated by its frequency response above 3 rad/s, where the rod inertia dominates the system response. To obtain the appropriate calibration constant, the mass "measured" by the high-frequency response can be compared to the mass obtained using a conventional scale.

Surface Rheology Measurements. With this device, the dynamic surface modulus, $G_s^*(\omega)$, is measured and is defined as the proportionality factor between the stress and the strain

$$\sigma_s e^{i\omega t} = G_s^*(\omega)\gamma_0 e^{i[\omega t - \delta(\omega)]} \tag{4}$$

where σ_s is the amplitude of the applied sinusoidal stress with frequency ω and γ_0 is the amplitude of the resultant strain at the same frequency ω that lags the stress by a phase angle $\delta(\omega)$. Note that $G_s^*(\omega)$ is a complex number. σ_s is equal to the amplitude of the force on the rod divided by $2L$ since the *interfacial* drag is symmetrically applied along the length of the rod. γ_0 is the amplitude of the rod displacement divided by the distance between the rod and the glass slide, W. By rearranging eq 4 and solving for $G_s^*(\omega)$, we can directly determine the real and imaginary components of the dynamic modulus

$$G_s^*(\omega) = \frac{\sigma_s}{\gamma_0} e^{i\delta(\omega)} = G_s'(\omega) + iG_s''(\omega) \tag{5}$$

where $G_s'(\omega)$ is the surface storage modulus and $G_s''(\omega)$ is the surface loss modulus. Here it is important to emphasize that the ability to create a sinusoidal flow field allows the determination of the phase difference, δ, from which the storage and loss modulus can be calculated. When the film is purely elastic $\delta = 0°$, and when it is purely viscous $\delta = 90°$. From eq 5, it is readily observable that the ratio of the storage and loss modulus is $\tan \delta = G_s''(\omega)/G_s'(\omega)$, which can be used as a measure of the ratio of the elastic to viscous nature of the monolayer. Similarly, a dynamic viscosity, $\mu_s^*(\omega)$, is commonly used to describe the flow behavior of complex materials and may be easily derived from the dynamic surface modulus

$$\mu_s^*(\omega) \equiv \mu_s'(\omega) - i\mu_s''(\omega) = \frac{G_s^*(\omega)}{i\omega} = \frac{G_s''(\omega)}{\omega} - i\frac{G_s'(\omega)}{\omega} \tag{6}$$

where $\mu_s'(\omega)$ and $\mu_s''(\omega)$ are the real and imaginary parts, respectively.

The response measured with a monolayer, however, contains contributions from the system (water drag, surface curvature, rod inertia, etc.) as well as the interface. The simplest way to decouple these two contributions is to assume that they are additive, which gives the following equation for the dynamic surface modulus:

$$G_s^* = \frac{w}{2L}\left(\frac{1}{AR_{monolayer}}e^{-i\delta_{monolayer}}\right) = \frac{w}{2L}\left(\frac{1}{AR_{meas}}e^{-i\delta_{meas}} - \frac{1}{AR_{system}}e^{-i\delta_{system}}\right) \quad (7)$$

In reality, the coupling between the subphase and the surface is more complicated since a stress applied to the surface may be dissipated into the subphase instead of through the film. If this is indeed the case, then the velocity profile is not necessarily linear but will decay to zero as it approaches the wall, where no slip is assumed. To avoid this, a smaller gap can be chosen to increase the stress in the film so that the surface stress dominates over the subphase stress.

An experimental Boussinesq number, Bo_{exp}, can be defined that takes into account the response of the instrumentation and the subphase:

$$Bo_{exp} \equiv \frac{AR_{system}}{AR_{meas}} \quad (8)$$

When Bo_{exp} is large, these system effects are negligible and there is no need to subtract the response of the needle to a clean water surface (eq 7). For both the fatty alcohol and the polymer−rod solutions studied here, $Bo_{exp} > 100$ and no subphase subtraction was done.

Method for Rheological Experiments. For each measurement, the monolayers were spread onto a clean water surface, with the rod and glass slides already placed in the trough. Note that the definition of the dynamic modulus (in eq 5) assumes that the relationship between surface stress and strain is linear. Before measuring the frequency dependence of $G_s^*(\omega)$, the sample is subjected to a strain sweep to ensure that the measurements are made in the linear regime. The strain is varied at a constant frequency to verify that the rheology is independent of the amount of deformation. Once the linear region was determined, a frequency sweep was conducted from 0.1 to 10 rad/s to probe the time scales of the film deformation behavior.

Brewster Angle Microscopy. A custom-made Brewster angle microscope (BAM) was used to image the morphology of the monolayer. P-polarized light from a 10-mW argon laser beam was incident at the Brewster angle (53.1° for an air−water interface), resulting in no light being reflected from a monolayer-free interface. When a monolayer was present, light was reflected, with variations in intensity arising from different molecular orientations. A 50-mm planoconvex lens was used to magnify the reflected light, and an analyzer was used to enhance contrast. The resulting image was recorded with a CCD camera.[26,27]

Materials. A monolayer mixture of a rodlike polymer and a fatty alcohol was used in this investigation. The polymer used was the "hairy-rod" polymer phthalocyaninatopolysiloxane (PcPS).[28] It has a highly rigid structure with a length of 34 nm and a width of 1.9 nm. The polymer had an average molecular weight of 59 500 and a degree of polymerization (DP) of 100 but was highly polydisperse. Eicosanol (C_{20}) (Sigma) was the fatty alcohol used. Mixtures of the hairy-rod polymer PcPS with eicosanol were made in chloroform with concentrations varying from 0 to 7.3 mol % PcPS monomer. All monolayers were spread using a microsyringe (Hamilton, Reno, NV) on a Milli-Q water subphase (18 MΩ·cm resistivity) held at a constant temperature of 22 ± 0.1 °C.

Results and Discussion

Isotherms. The isotherms of monolayer solutions of PcPS in eicosanol are presented in Figure 5. The low-pressure phase is the L_2' phase, and the high-pressure phase is called the LS_I phase, following the naming convention of Kaganer et al.[18] The presence of polymer in the film does not significantly alter the shape of the isotherm or any of the transitions. The mean area increases as polymer is added, verifying that the polymer is incorporated into the monolayer. These isotherms can be used to estimate the area per molecule for both eicosanol and the PcPS rods. In Figure 6, the average area (extrapolated to zero surface pressure) is plotted against monomer concentration. The intercept is the average area per eicosanol molecule, and the slope (when multiplied by 100) is the difference in areas of the eicosanol and PcPS monomer. The average area for eicosanol is 21.4 Å^2/molecule, which agrees with the literature,[29] and for the PcPS monomer it is 67.2 Å^2/monomer or 6720 Å^2/rod (for a degree of polymerization of 100). This is in acceptable agreement with the value of 6460 Å^2/rod calculated from the molecular dimensions of PcPS stated above.

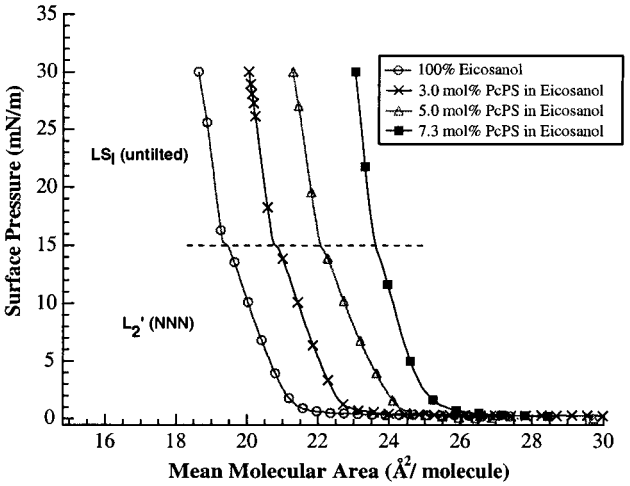

Figure 5. Isotherms for PcPS−eicosanol solutions at 22 °C. The area per molecule is reported as an average area for the eicosanol and PcPS monomers. As polymer is added, the area where the surface pressure lifts off increases, indicating that the polymer is incorporated into the monolayer and does not get squeezed out. There are two phases at this temperature: a low-pressure L_2' phase below 15 mN/m and a high-pressure LS_I phase above 15 mN/m. Every 10th data point is labeled to prevent obscuring the isotherm features.

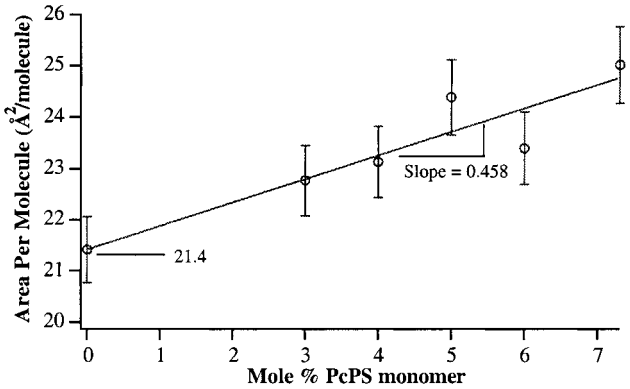

Figure 6. Average molecular area where the surface pressure lifts off against the concentration of monomer (±3% error bars are used). The data here can be used to estimate the area of a PcPS rod, which agrees well with the value calculated from molecular dimensions.

Surface Rheology of Eicosanol. The surface storage and loss moduli for eicosanol at 22 °C are plotted against surface pressure in Figure 7. At low surface pressures ($\Pi < 15$ mN/m), the film is very viscous, yet at higher surface pressures ($\Pi > 15$ mN/m), the film becomes more

(26) Henon, S.; Meunier, J. *Rev. Sci. Instrum.* **1991**, *62*, 936.
(27) Friedenberg, M. C.; Fuller, G. G.; Frank, C. W.; Robertson, C. R. *Langmuir* **1996**, *12*, 1594.
(28) Schwiegk, S.; Vahlenkamp, T.; Xu, Y.; Wegner, G. *Macromolecules* **1992**, *25*, 2513.
(29) Overbeck, G. A.; Hönig, D.; Möbius, D. *Langmuir* **1993**, *9*, 555.

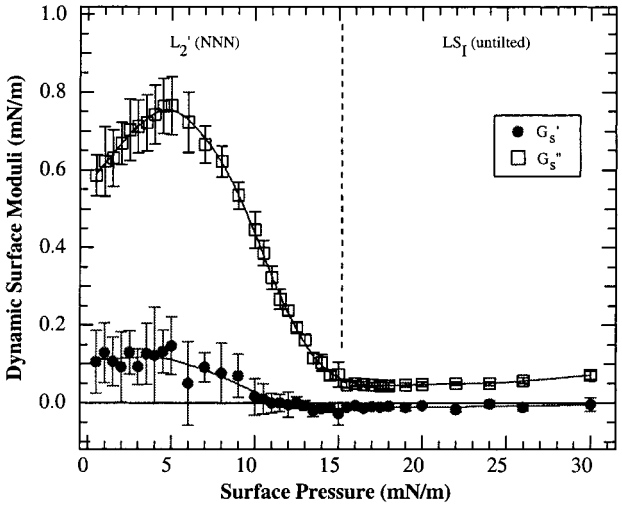

Figure 7. Surface storage and loss moduli for eicosanol as a function of surface pressure. The pressure-induced liquefaction observed at the $L_2'-LS_I$ transition[6,30] is due to the required increase in entropy as the monolayer is compressed because $d\Pi_{eq}/dT$ is negative along the $L_2'-LS_I$ coexistence boundary. The maximum observed within the L_2' phase is different from the maximum observed in the L_2 phase of heneicosanoic acid.[19] Heneicosanoic acid is hexagonally packed at a unique pressure within the L_2 phase, which may be correlated to the maximum in G_s'', but the L_2' phase of eicosanol never attains this hexagonal structure. The maximum we observe here must have a different, unknown, origin.

compliant. The reduction of G_s'' with surface pressure within the L_2' phase ($\Pi > 6$ mN/m) agrees with other workers[6,30] and is related to the reduction of molecular tilt angle in the monolayer to attain higher surface densities.

As the pressure is increased from zero, G_s'' increases and then decreases within the L_2' phase with a maximum observed at around 6 mN/m. No apparent changes in surface morphology were observed, however, when examined with the BAM near these pressures. Ghaskadvi et al.[19] have observed a similar maximum in their rheological studies of heneicosanoic acid (C_{21}). In their work, a maximum in G_s'' within the L_2 phase (alkyl chains with NN tilt) was correlated with the state when the headgroups are arranged on a regular (undistorted) hexagonal lattice. Unlike fatty acids, fatty alcohols lack a phase where the chains are tilted toward their nearest neighbors.[31,32] X-ray diffraction data on heneicosanol (C_{21})[33] showed no hexagonal transition within the L_2' phase; thus, the maximum we observed here is not correlated with the same structural transition. We are currently examining this system further to determine how its rheological response changes with temperature to better understand the nature of this maximum.

We also monitored this pressure-induced liquefaction process with Brewster angle microscopy as the film was compressed from the L_2' phase to the LS_I phase (Figure 8). A polydomain structure due to varying tilt azimuth is evident in the L_2' phase, but the LS_I phase had no observable contrast since the molecules are perpendicular to the interface. As the film was expanded, the nucleation and growth of these domains could be observed, providing evidence that the transition is first-order. In general, the crystal size was inversely related to the rate of expansion, but since this was not our main aim, it was not studied extensively. Our BAM results agree with the more extensive BAM studies of eicosanol by Overbeck et al.[29]

The general phase diagram for fatty acids proposed by Kaganer et al.[18] along with experimental data on fatty acids and alcohols[29,31,32,34] illustrates that the $L_2'-LS_I$ coexistence boundary has a negative $d\Pi_{eq}/dT$. The Clapeyron equation for pure substances states that the slope of the phase coexistence line is equal to the ratio of the change in entropy ($\Delta S_{\alpha\rightarrow\beta}$) with the change in area ($\Delta A_{\alpha\rightarrow\beta}$) during the transition:

$$\frac{d\Pi_{eq}}{dT} = \frac{S_\beta - S_\alpha}{A_\beta - A_\alpha} = \frac{\Delta S_{\alpha\rightarrow\beta}}{\Delta A_{\alpha\rightarrow\beta}} \qquad (9)$$

Since $d\Pi_{eq}/dT < 0$, when compressing the film to go from the L_2' phase to the LS_I phase ($\Delta A_{L_2'\rightarrow LS_I} < 0$), the entropy must increase, $\Delta S_{L_2'\rightarrow LS_I} > 0$. The phase behavior of water exhibits a similar phenomenon since dP_{eq}/dT is negative along the solid−liquid coexistence curve. When water is compressed from a solid to a liquid, the entropy increases, with a subsequent decrease in viscosity. The viscosity decreases since the water takes on a more random, less ordered structure in the liquid state. An analogous phenomenon occurs in the eicosanol monolayer. As it is compressed from the L_2' phase (where the molecules are positioned on a distorted hexagonal lattice and tilted toward their next-nearest neighbors) to the LS_I phase (where the molecules are untilted and positioned on a hexagonal lattice but have additional rotational freedom about their chain axis), the entropy is increased. As a result, the surface viscosity decreases across this phase boundary due to the loss of order within the film.

In the LS_I phase, G_s'' is independent of surface pressure, a result of the low compressibility of the high-pressure phase. The morphology of the LS_I phase is unobservable with BAM since there is no molecular tilt, which is consistent with X-ray diffraction results on heneicosanol.[31,33] The film is predominantly viscous and has a negligible amount of elasticity.

The oscillation frequency of the rod was varied from 0.1 to 10 rad/s at a surface pressure of 30 mN/m with the results presented in Figure 9. G_s'' is larger than G_s', and at higher frequencies, G_s' eventually becomes undetectable as the phase difference between the stress and the strain approaches 90°. For an ideal Newtonian-like interface, the surface loss modulus scales with frequency. Indeed, this is the case for eicosanol, where the frequency exponent is 1.1. This is in agreement with previous observations made with fatty alcohols in this phase.[35] From these results, we conclude that eicosanol forms a Newtonian interface with a surface viscosity of 0.03 mN·s/m[36] and the rheology is independent of pressure at 30 mN/m. Since the monolayer behaves as a Newtonian film over a broad range of surface pressures, it was used as a solvent for dispersing a rigid-rod polymer to study its liquid-crystalline phases at 30 mN/m. The pressure independence of this phase also makes it a viable candidate for a surface rheology standard for comparing mechanical results between different surface rheometers.

(30) Copeland, L. E.; Harkins, W. D.; Boyd, G. E. *J. Chem. Phys.* **1942**, *10*, 357.
(31) Shih, M. C.; Durbin, M. K.; Malik, A.; Zschack, P.; Dutta, P. *J. Chem. Phys.* **1994**, *101*, 9132.
(32) Fischer, B.; Teer, E.; Knobler, C. M. *J. Chem. Phys.* **1995**, *103*, 2365.
(33) Shih, M. C.; Bohanon, T. M.; Mikrut, J. M.; Zschack, P.; Dutta, P. *J. Chem. Phys.* **1992**, *97*, 4485.
(34) Harkins, W. D.; Copeland, L. E. *J. Chem. Phys.* **1942**, *10*, 272.
(35) Miyano, K.; Abraham, B. M.; Ketterson, J. B.; Xu, S. Q. *J. Chem. Phys.* **1983**, *78*, 4776.
(36) The SI equivalent to a surface Poise, sP, which has units of g/s, is 1 mN·s/m.

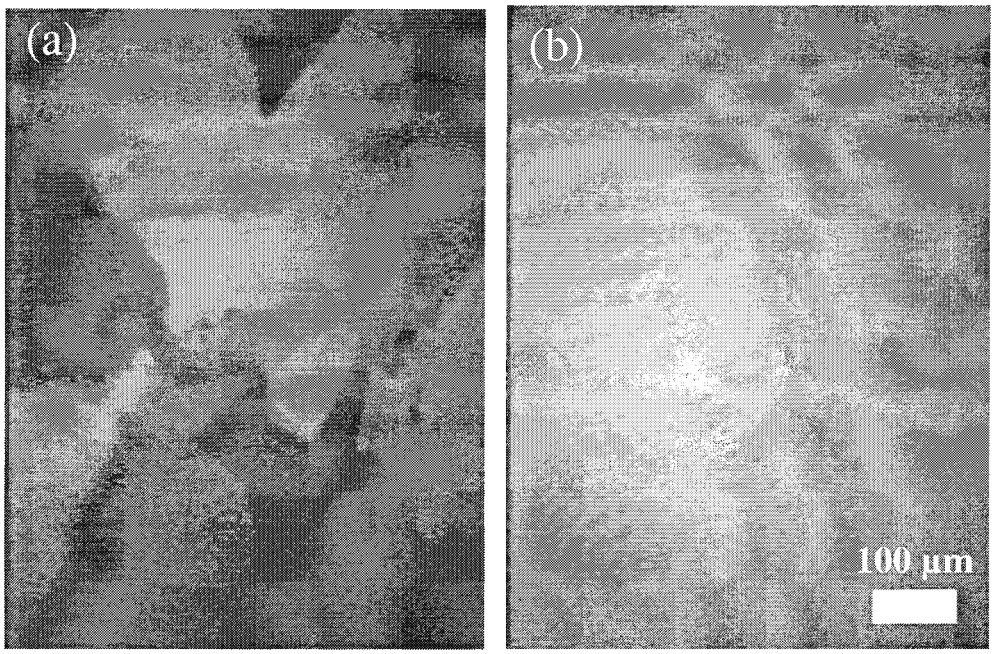

Figure 8. BAM images of eicosanol in the (a) L_2' phase and the (b) LS_I phase. The image of the L_2' phase shows polydomain texture arising from the NNN tilt of the alkyl chains. No texture is observed in the LS_I phase because the molecules are normal to the interface.

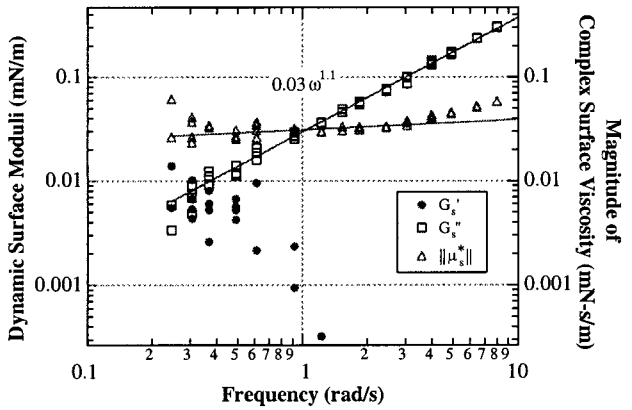

Figure 9. Frequency dependence of the dynamic moduli and complex viscosity for eicosanol at 22 °C and 30 mN/m. G_s'' is proportional to ω, and the magnitude of the complex viscosity is independent of ω, implying that the surface is Newtonian-like.

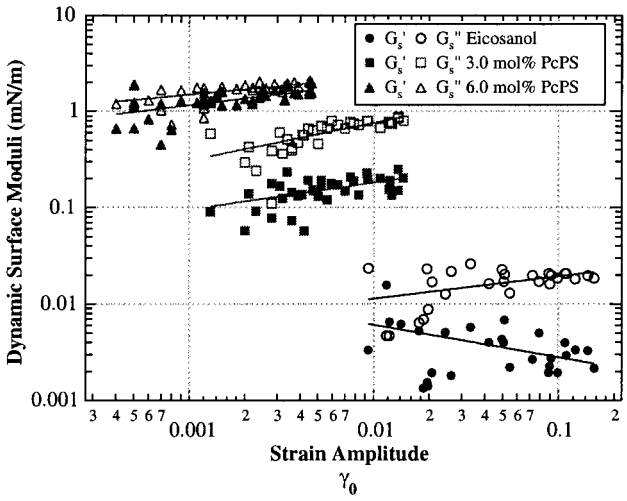

Figure 10. Dependence of the dynamic surface moduli with strain at $\omega = 0.63$ rad/s and $\pi = 30$ mN/m. For all the polymer concentrations studied, the moduli exhibited a weak dependence on strain, implying that our measurements were conducted in the linear viscoelastic region.

Surface Rheology of PcPS in Eicosanol. The dependence of the surface moduli on strain amplitude is shown in Figure 10 for eicosanol and solutions of PcPS (3 and 6 mol %) in eicosanol. The data taken for eicosanol are shifted to higher strains because it is less viscous. Since the device is really a constant-stress rheometer, the stress is varied and the resultant strain is measured. All the samples have a small dependence on strain, implying that the applied deformations do not drastically perturb the structure of the film. Thus, the *linear* viscoelastic properties of the film are measured.

The results of frequency sweeps of the PcPS solutions in eicosanol are shown in Figures 11 and 12. Notice that at 3 mol % PcPS monomer, the magnitude of the surface modulus, $||G_s^*||$, increases by 2 orders of magnitude compared to the polymer-free response in Figure 9. By reexamining the isotherms in Figure 5, we find that the 3 mol % PcPS isotherm is displaced to the right of the pure eicosanol but the phase transitions and general shape are the same. The frequency dependence of both the storage and loss moduli, however, changes significantly. Both moduli scale with frequency to the ~0.6 power for the 3.0 mol % PcPS monomer film, whereas the loss modulus for eicosanol is proportional to frequency. Clearly the addition of a small amount of rigid-rod polymer has a more dramatic effect on the surface rheology than it does on the isotherm behavior. The rheology may be a more sensitive measure of the state of the monolayer.

When the concentration of rods at the surface exceeds 5 mol %, the rods undergo an isotropic−nematic phase transition where they are oriented at equilibrium due to an increase in rod-rod interactions. This value has been determined from linear dichroism measurements done in our laboratory.[16] Below this transition, the film is isotropic. As the polymer concentration is increased in the isotropic phase (Figures 11 and 12), $||G_s^*||$ increases, with G_s' increasing more rapidly than G_s''. Rod-rod interactions increase with concentration, and more energy is capable of being stored as potential energy from excluded volume

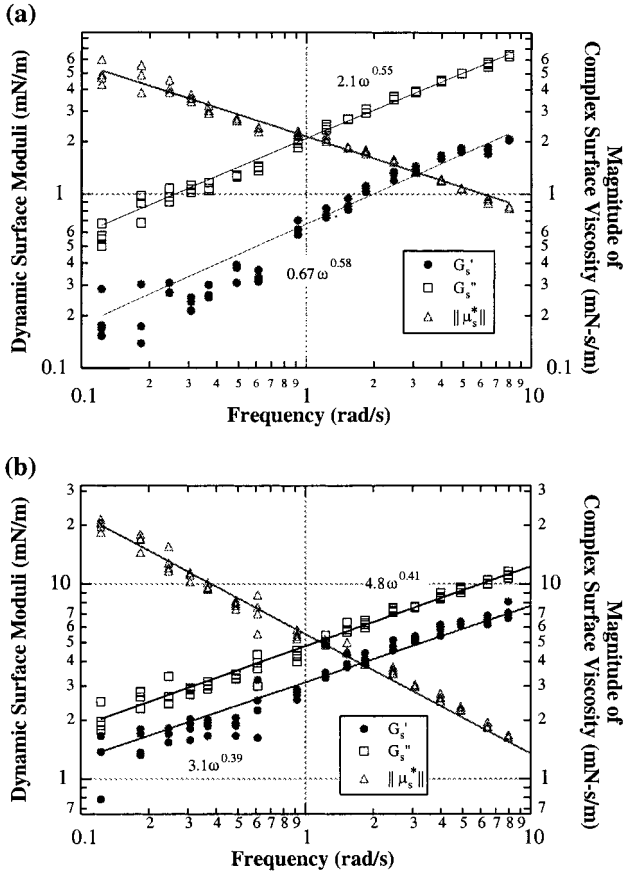

Figure 11. Frequency dependence of the dynamic moduli and complex viscosity for (a) 3.0 mol % PcPS monomer and (b) 5.0 mol % PcPS monomer. In comparison to Figure 9, the presence of the polymer increases the surface viscosity 100-fold (0.03−2.2 mN·s/m at $\omega = 1$ rad/s) and makes the interface non-Newtonian. Increasing the polymer rod concentration to 5 mol % causes the elastic contribution to increase and lessens the frequency dependence.

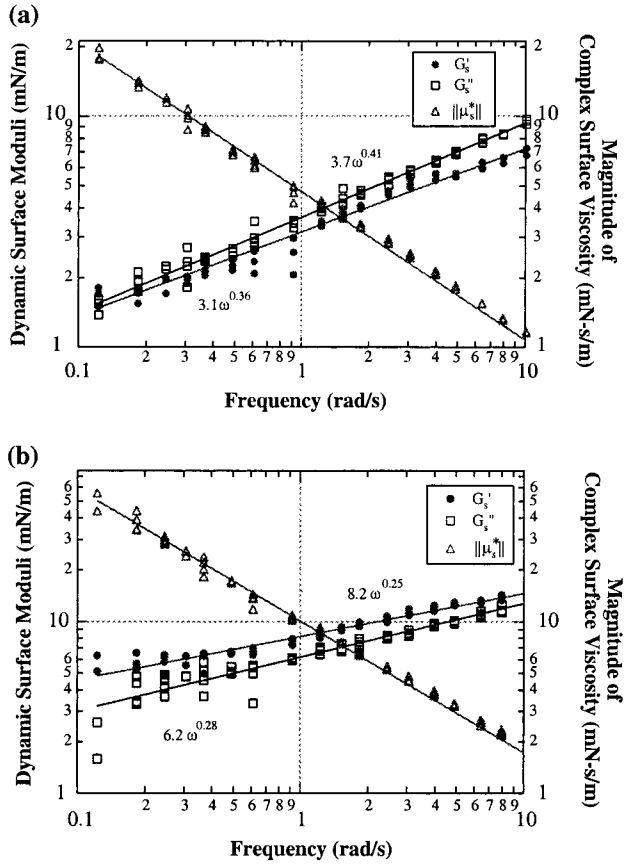

Figure 12. Frequency dependence of the dynamic moduli and complex viscosity for (a) 6.0 mol % PcPS monomer and (b) 7.3 mol % PcPS monomer. Further increases in polymer rod concentration cause the film to undergo an isotropic−nematic transition. A rheological transition is observed here as the film changes from being viscous, with $G_s'' > G_s'$ in a, to elastic, $G_s' > G_s''$ in b. The frequency dependence also decreases as the film behaves like an ideally elastic film.

effects, resulting in the larger increase in G_s'. Eventually, as the nematic transition is crossed, G_s' overtakes G_s'' (Figure 12).

The mole fraction of monomer, $x_{monomer}$, can be converted to the mole fraction of rods, x_{rods}, using the formula

$$x_{rods} = \frac{\frac{x_{monomer}}{DP}}{\frac{x_{monomer}}{DP} + (1 - x_{monomer})} \qquad (10)$$

To convert to the number concentration of rods, c, x_{rods} is divided by the average area per molecule, which depends on the amount of polymer in the monolayer and typically ranges from 21 to 26 Å^2/molecule. Knowledge of the concentration in terms of a number density is useful when trying to compare our results to molecular theories of polymer dynamics, such as the polymer liquid-crystal model of Doi[21] and Hess.[22] In these models, a dimensionless concentration is used, defined as $U = cL_p^2$, where L_p is the length of the rigid rod, which is 850 nm for the PcPS rigid rods used here.

Table 1 summarizes the frequency response data and includes the dimensionless concentrations for each mole fraction. The dimensionless concentration at which the transition is observed, $U = 2.53$, agrees with the findings of Maffettone and co-workers:[17,20] Using Maier−Saupe and Onsager models for the nematic potential, they predicted the isotropic−nematic transition to occur at $U = 2-2.35$.

Table 1. Summary of Frequency Response Data

$x_{monomer}$, mol % PcPS	c^a	$U^b = cL_p^2$	at 1 rad/s		exponent	
			G_s*, mN/m	tan δ	G_s'	G_s''
0	0	0	0.03	30		1.1
3.0	1290	1.49	2.2	3.1	0.58	0.55
4.0	1740	2.01	3.4	1.9	0.39	0.49
5.0	2190	2.53	5.7	1.5	0.39	0.41
6.0	2660	3.07	4.8	1.2	0.36	0.41
7.3	3280	3.79	10	0.76	0.25	0.28

[a] Number of PcPS rods per mm^2 of surface. [b] Dimensionless concentration.

In Figure 13, the magnitude of the complex viscosity, $||\mu_s^*||$, is plotted vs polymer concentration, and there appears to be a local maximum near 5 mol % PcPS, where an isotropic-to-nematic phase transition occurs. The viscosity data in the isotropic phase are best fit by a curve of the form $C_1 x_{monomer}^2$ drawn through the points, in contrast to the $x_{monomer}^3$ dependence predicted by the Doi−Hess model when considering the elastic component of the stress.[21,23] The two-dimensional nature of the film may alter our observed concentration dependence in the isotropic phase, resulting in a higher contribution from the viscous component of the stress. A curve that considers both the elastic and viscous components of the stress takes the form of $C_2 x_{monomer} + C_3 x_{monomer}^3$ and leads to a better fit, but more data are needed to confirm this. The

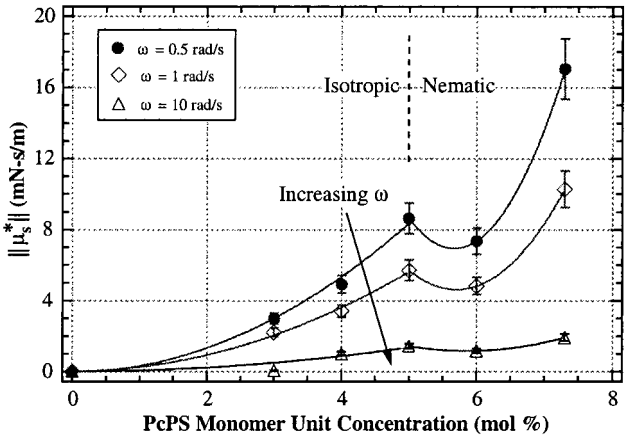

Figure 13. Dependence of the magnitude of the complex surface viscosity with polymer rod concentration and frequency. Below the isotropic−nematic transition, the viscosity increases with concentration and is shear thinning. Above the transition, the viscosity does not decrease, as one would expect for steady shear flow, because the applied strains are not large enough to align the rods with this oscillatory shear experiment.

maximum has been observed and predicted for solutions of rigid rods in three dimensions[21,24,25] for steady and oscillatory shear flows. In these systems, above the transition, the viscosity typically drops to low values and then begins to gradually increase at higher concentrations. This increase with concentration in the nematic phase arises from increased rod-rod interactions. However, in this study, the initial rod orientation was not specified since no preshearing can be done with the present device. The small decrease in $||\mu_s^*||$ within the nematic phase is not as large as observed in the three-dimensional case since there is not an appreciable amount of orientation induced in the flow direction. The response at different deformations, presented in Figure 10, implies that the flow was not strong enough to reorient the rigid rods.

The strength of the flow can be characterized by a rotary Peclet number, Pe_r, defined as

$$Pe_r = \frac{\text{diffusion time scale}}{\text{flow time scale}} = \frac{\gamma_0 \omega}{D_r} \qquad (11)$$

where D_r is the rotational diffusivity of the rods. With D_r[17] of approximately 0.03 s^{-1} and γ_0 equal to 0.006, Pe_r ranges from 0.02 to 2 over the frequencies studied. Since Pe_r is order one or less, the flow strength is not large enough to couple with the orientation of the rods. If Pe_r were much larger than one, the rheology would be highly nonlinear, which would not allow the measurement of the linear viscoelastic parameters.

By examining this rigid-rod solution, we have provided evidence that the rheological response exhibits the correct trends and that this device is appropriate for studying rheological transitions in Langmuir monolayers. All our previous work[16,17] focused on measuring the order parameter and director orientation from measurements of the optical anisotropy (dichroism) when subjected to shear and planar extensional flow. Unfortunately, with these flow cells, you cannot measure the viscosity or the elasticity—the increase in torque to drive the flow is negligible. With this instrument, we can measure the storage and loss moduli at different rigid-rod concentrations, and this information can be used to complement our dichroism data.

Summary

We have constructed a device to probe the surface rheology of Langmuir films at the air−water interface. The instrument moves a magnetized rod floating at the surface by applying a force generated from a magnetic field gradient. The present design allows us to subject the monolayer to oscillatory flow and to vary the forcing frequency from 0.1 to 10 rad/s. We plan to modify the instrument in the near future to conduct creep experiments, where a constant stress is applied on the film and the resulting rod motion is followed. An investigation of the surface rheology of eicosanol demonstrated that the film behaved as a Newtonian surface with surface viscosity 0.03 mN·s/m in the high-pressure LS_I phase. As a rigid-rod polymer was added to the film, the magnitude of the surface modulus, $||G_s^*||$, increased by a factor of 100 and showed a local maximum near 5 mol % PcPS monomer, the location of an isotropic−nematic phase transition. Also, near this transition, a crossover from fluidlike behavior to elastic-like behavior was observed. The detection of both the isotropic−nematic phase transition in the rigid-rod polymer solutions and the L_2'−LS_I phase transition in eicosanol demonstrates that our rheometer is capable of detecting microstructural changes in a Langmuir monolayer. In addition to the model monolayer systems discussed here, the mechanical surface rheology of other, more complex amphiphiles are currently under investigation. For example, the instrument is being used to understand the formation of a physical network in poly(ethylene glycol) lipopolymers, to study the kinetics of cross-linking a polymerizable lipid, to determine a relaxation time for a flexible polymer, and to examine the kinetics of protein adsorption to an air−water interface.

Acknowledgment. We thank Lew Nunnely at IBM in San Jose, CA, for loaning us a pair of Helmholtz coils during our preliminary work and Prof. C. M. Knobler for useful discussions. This work was funded in part by the National Science Foundation Materials Research Science and Engineering Center Program (DMR-9400354) through the Center on Polymer Interfaces and Macromolecular Assemblies (CPIMA) and the NIH Biotechnology Training Program (Grant 5 T32 GMO8412-07).

Glossary of Terms

a = radius of magnetic rod, length

A_c = characteristic area, the area of contact the rheological probe has with the subphase, area

AR = amplitude ratio, defined as the distance the rod is displaced per unit force, length/force

AR_{meas} = amplitude ratio measured with a monolayer present, length/force

$AR_{monolayer}$ = amplitude ratio determined for a monolayer, after subtracting system effects, length/force

AR_{system} = amplitude ratio measured for a monolayer-free interface, length/force

Bo = Boussinesq number; the ratio of the drag from the surface to the subphase

Bo_{exp} = experimental Boussinesq number, which is the ratio of AR_{system}/AR_{meas}, dimensionless

c = surface concentration of rodlike polymer, number/area

d = damping constant for the system, force·time/length

D_r = rotational diffusivity, 1/time

G_s^* = dynamic surface modulus, generally a complex number, force/length

$||G_s^*||$ = magnitude of G_s^*, force/length

G_s' = dynamic surface storage modulus, real part of G_s^*, force/length

G_s'' = dynamic surface loss modulus, imaginary part of G_s^*, force/length
k = system compliance, force/length
L = length of magnetic rod, length
L_c' = characteristic length for the velocity gradient in the surface, length
L_c'' = characteristic length for the velocity gradients in the underlying subphase, length
L_m = length of a monomer unit, length
L_p = length of the rodlike polymer, length
m = mass of rod, mass
P_c = characteristic contact perimeter of the rheological probe with the interface, the length of the probe that is in contact with the surface, length
Pe_r = rotary Peclet number, the ratio of the diffusion time scale to the flow time scale, dimensionless
T = temperature, °C
U = dimensionless rigid-rod concentration
U^* = dimensionless rigid-rod concentration above which the rods are aligned at equilibrium (nematic)
V = characteristic velocity of rod, length/time
W = distance between rod and stationary wall, length
$x_{monomer}$ = mole fraction of monomer units at the interface
x_{rods} = mole fraction of rods at the interface
δ = phase difference between the strain and stress, angle
δ_{meas} = phase difference measured between the rod position and the applied stress with a monolayer present, angle
$\delta_{monolayer}$ = phase difference calculated between the strain and the applied stress for a monolayer, after subtracting system effects, angle
δ_{system} = phase difference measured between the rod position and the applied stress for a monolayer-free surface, angle
γ_0 = amplitude of strain
$\dot{\gamma}_0$ = amplitude of strain rate, 1/time
μ = subphase viscosity, force·time/length^2
μ_s = surface viscosity, force·time/length
μ_s^* = complex surface viscosity, generally a complex number, force·time/length
$||\mu_s^*||$ = magnitude of μ_s^*, force·time/length
μ_s' = real part of the complex viscosity, force·time/length
μ_s'' = imaginary part of the complex viscosity, force·time/length
Π = surface pressure, force/length
σ_s = surface stress, force/length
ω = frequency of the applied force and resultant strain, rad/s

LA980465R